

A Systematic Investigation of the Relaxation Properties of Fe(III)-EDTA Derivatives and Their Potential as MRI Contrast Agents

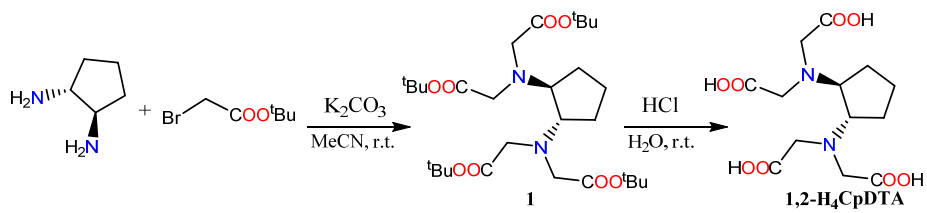
Rocío Uzal-Varela,[†] Fátima Lucio-Martínez,[†] Alessandro Nucera,[‡] Mauro Botta,^{*,‡} David Esteban-Gómez,[†] Laura Valencia,[§] Aurora Rodríguez-Rodríguez,^{*,†} and Carlos Platas-Iglesias[†]

[†] Universidade da Coruña, Centro de Investigacións Científicas Avanzadas (CICA) and Departamento de Química, Facultade de Ciencias, 15071, A Coruña, Galicia, Spain

[‡] Dipartimento di Scienze e Innovazione Tecnologica, Università del Piemonte Orientale “A. Avogadro”, Viale T. Michel 11, 15121 Alessandria, Italy.

[§] Departamento de Química Inorgánica, Universidade de Vigo, Facultad de Ciencias, 36310 Pontevedra, Spain

Figure S29: Cyclic voltammogram of $[\text{Fe}(\text{PDTA})]^-$ complex in aqueous solution in 0.15 M NaCl (3.0 mM, pH= 5.9), recorded at 10, 50, 100, 250, and 500 $\text{mV}\cdot\text{s}^{-1}$ (top); and plots of the linear dependence of anodic and cathodic peak currents with the square root of the scan rate (bottom).....	21
Figure S30: Cyclic voltammogram of $[\text{Fe}(\text{CBuDTA})]^-$ complex in aqueous solution in 0.15 M NaCl (2.3 mM, pH= 5.7), recorded at 10, 50, 100, 250, and 500 $\text{mV}\cdot\text{s}^{-1}$ (top); and plots of the linear dependence of anodic and cathodic peak currents with the square root of the scan rate (bottom).....	22
Figure S31: Cyclic voltammogram of $[\text{Fe}(\text{CBuDEDPA})]^+$ complex in aqueous solution in 0.15 M NaCl (1.5 mM, pH= 5.1), recorded at 10, 50, 100, 250, and 500 $\text{mV}\cdot\text{s}^{-1}$ (top); and plots of the linear dependence of anodic and cathodic peak currents with the square root of the scan rate (bottom).....	23
Figure S32: Speciation diagram calculated for the Fe(III)-PDTA ⁴⁻ using the equilibrium data reported in the literature. ¹	24
Table S2: Optimized Cartesian coordinates (Å) of the $[\text{Fe}(\text{EDTA})(\delta)(\text{H}_2\text{O})]^- \cdot 5\text{H}_2\text{O}$ system obtained with DFT calculations (0 Imaginary Frequencies).....	24
Table S3: Optimized Cartesian coordinates (Å) of the $[\text{Fe}(\text{EDTA})(\lambda)(\text{H}_2\text{O})]^- \cdot 5\text{H}_2\text{O}$ system obtained with DFT calculations (0 Imaginary Frequencies).....	25
Table S4: Optimized Cartesian coordinates (Å) of the $[\text{Fe}(t\text{-CDTA})(\delta)(\text{H}_2\text{O})]^- \cdot 5\text{H}_2\text{O}$ system obtained with DFT calculations (0 Imaginary Frequencies).....	26
Table S5: Optimized Cartesian coordinates (Å) of the $[\text{Fe}(t\text{-CDTA})(\lambda)(\text{H}_2\text{O})]^- \cdot 5\text{H}_2\text{O}$ system obtained with DFT calculations (0 Imaginary Frequencies).....	27
Table S6: Optimized Cartesian coordinates (Å) of the $[\text{Fe}(c\text{-CDTA})(\delta)(\text{H}_2\text{O})]^- \cdot 5\text{H}_2\text{O}$ system obtained with DFT calculations (0 Imaginary Frequencies).....	28
Table S7: Optimized Cartesian coordinates (Å) of the $[\text{Fe}(c\text{-CDTA})(\lambda)(\text{H}_2\text{O})]^- \cdot 5\text{H}_2\text{O}$ system obtained with DFT calculations (0 Imaginary Frequencies).....	30
Table S8: Optimized Cartesian coordinates (Å) of the $[\text{Fe}(\text{CpDTA})(\delta)(\text{H}_2\text{O})]^- \cdot 5\text{H}_2\text{O}$ system obtained with DFT calculations (0 Imaginary Frequencies).....	31
Table S9: Optimized Cartesian coordinates (Å) of the $[\text{Fe}(\text{CpDTA})(\lambda)(\text{H}_2\text{O})]^- \cdot 5\text{H}_2\text{O}$ system obtained with DFT calculations (0 Imaginary Frequencies).....	32
Table S10: Optimized Cartesian coordinates (Å) of the $[\text{Fe}(\text{PhDTA})(\text{H}_2\text{O})]^- \cdot 5\text{H}_2\text{O}$ system obtained with DFT calculations (0 Imaginary Frequencies).....	33
Table S11: Optimized Cartesian coordinates (Å) of the $[\text{Fe}(\text{CBuDTA})(\text{H}_2\text{O})]^- \cdot 5\text{H}_2\text{O}$ system obtained with DFT calculations (0 Imaginary Frequencies).....	34
References	35



Scheme S1: Synthesis of **1,2-H₄CpDTA**.

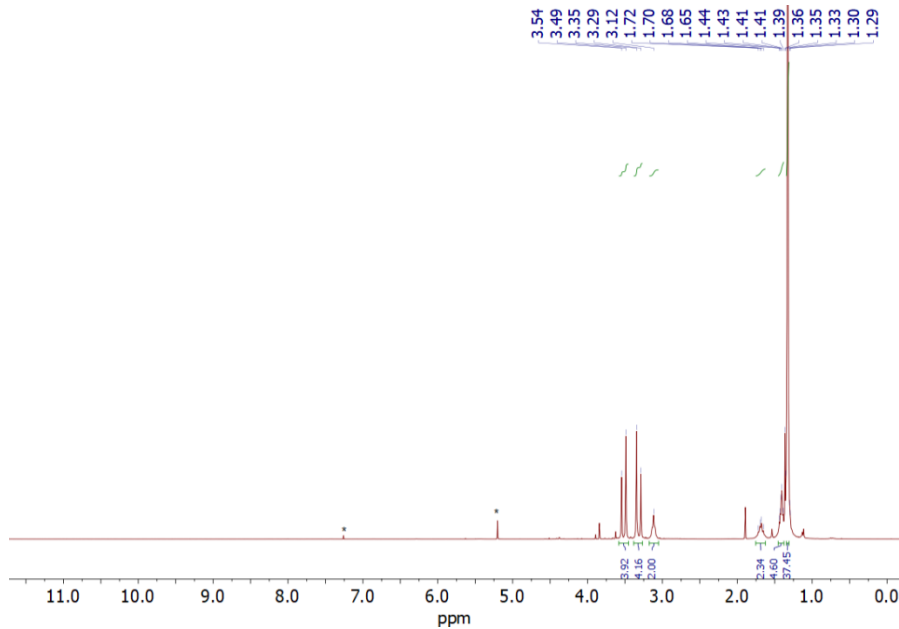


Figure S1: ¹H NMR spectrum of compound **1** (300 MHz, CDCl₃, 298 K).

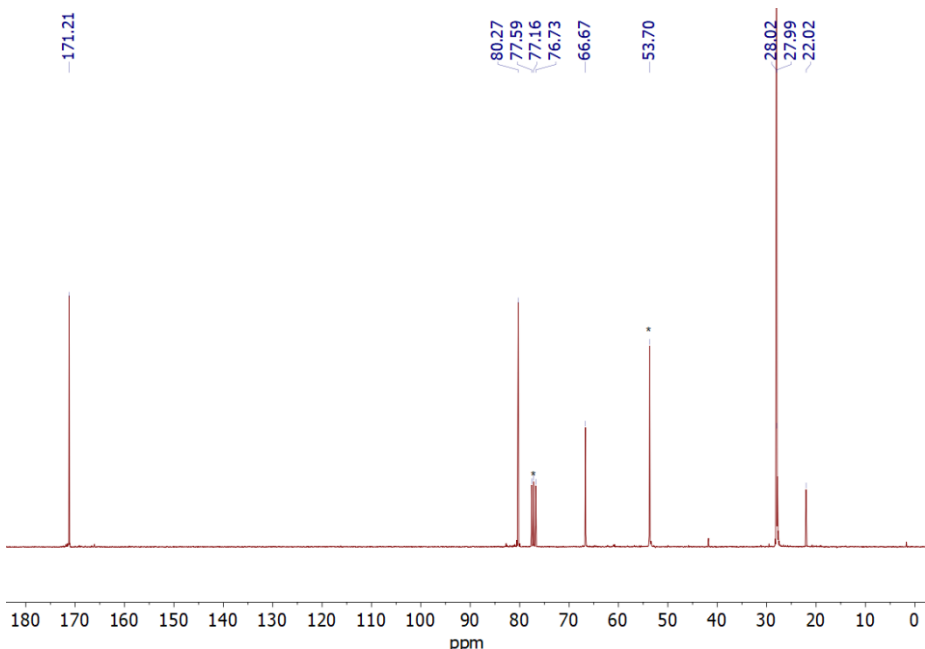


Figure S2: ¹³C NMR spectrum of compound **1** (75 MHz, CDCl₃, 298 K).

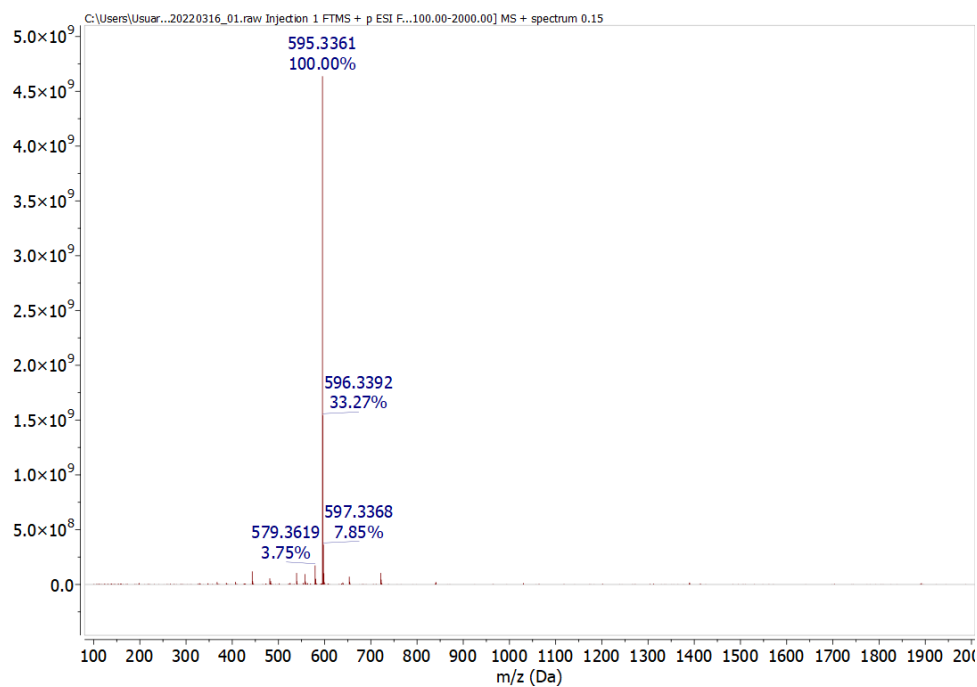


Figure S3: Experimental high resolution mass spectrum (ESI^+) of compound **1**.

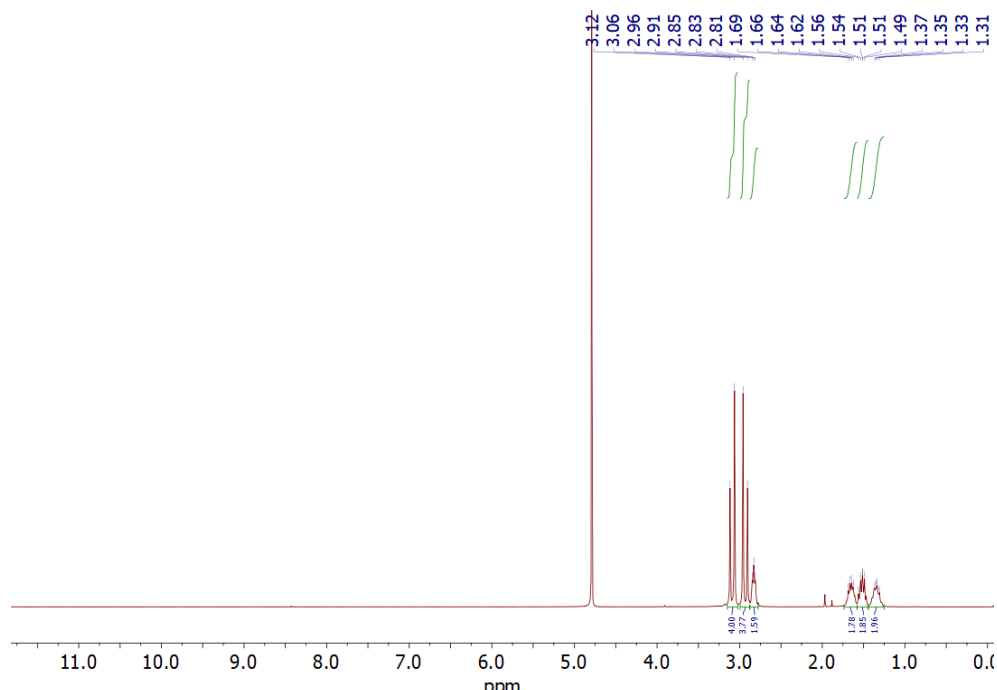


Figure S4: ^1H NMR spectrum of **1,2-H₄CpDTA** (300 MHz, D_2O , 298 K, pH 14).

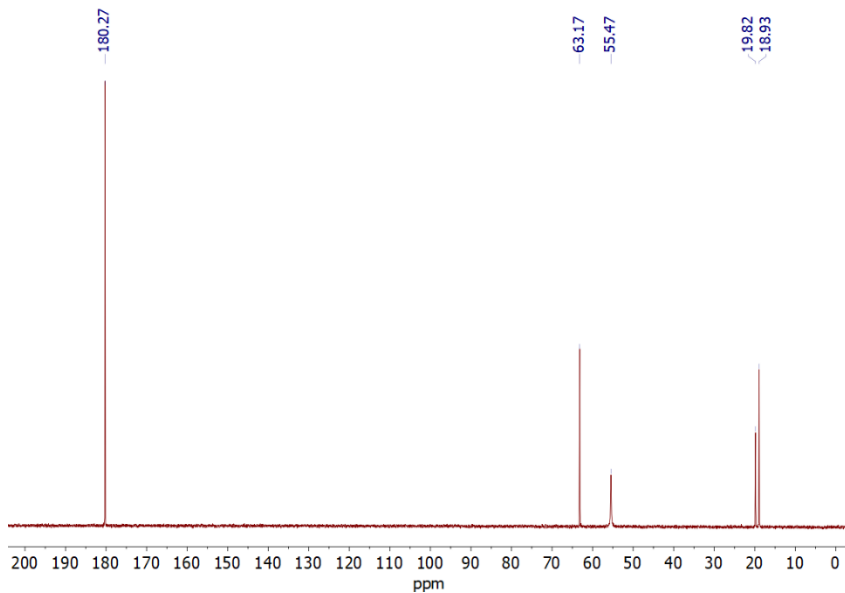


Figure S5: ^{13}C NMR spectrum of **1,2-H₄CpDTA** (75 MHz, D₂O, 298 K, pH 14).

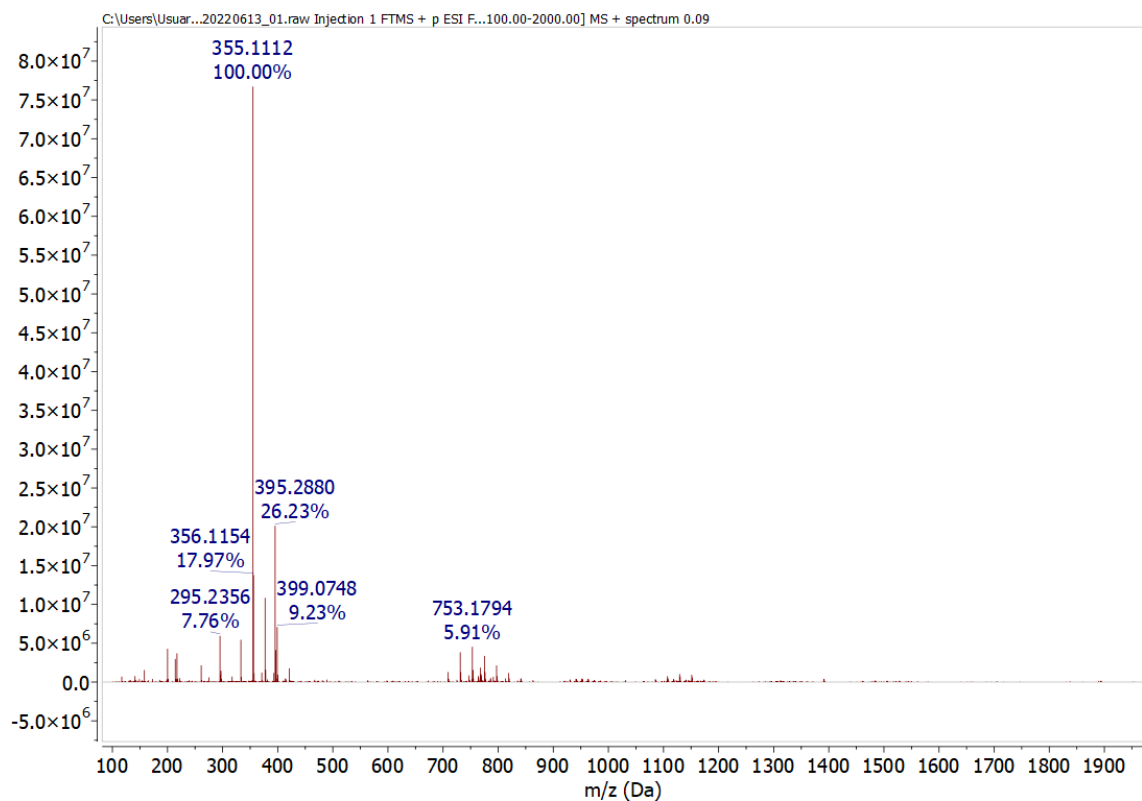
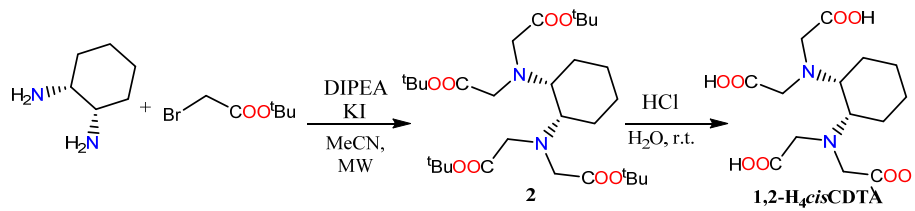


Figure S6: Experimental high resolution mass spectrum (ESI $^+$) of **1,2-H₄CpDTA**.



Scheme S2: Synthesis of **1,2-cis**-H₄CDTA.

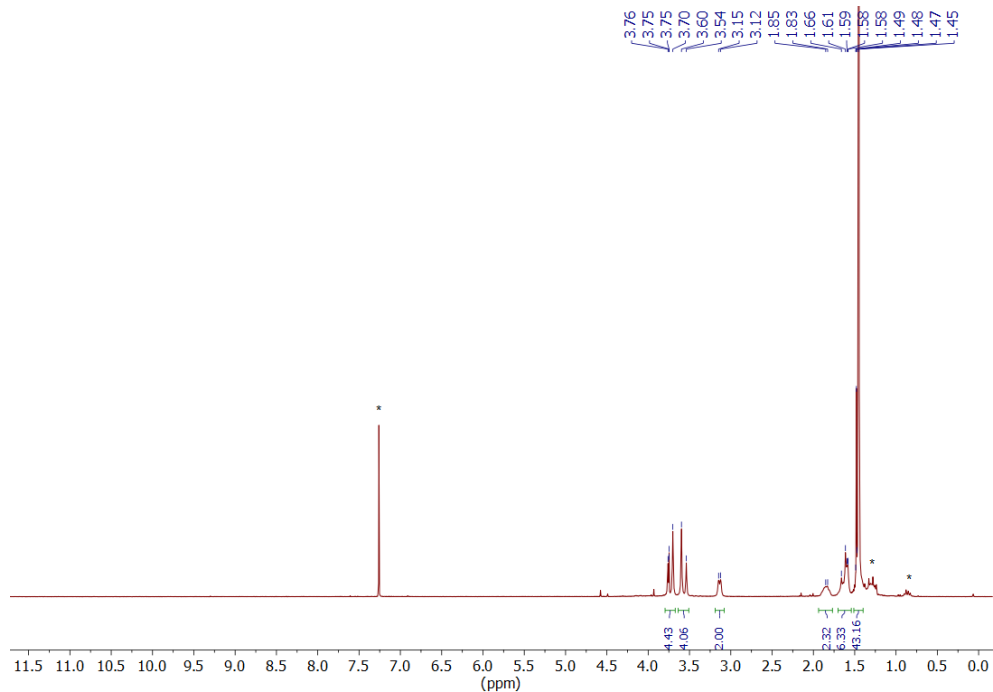


Figure S7: ¹H NMR spectrum of compound **2** (300 MHz, CDCl₃, 298 K). *Solvent residues

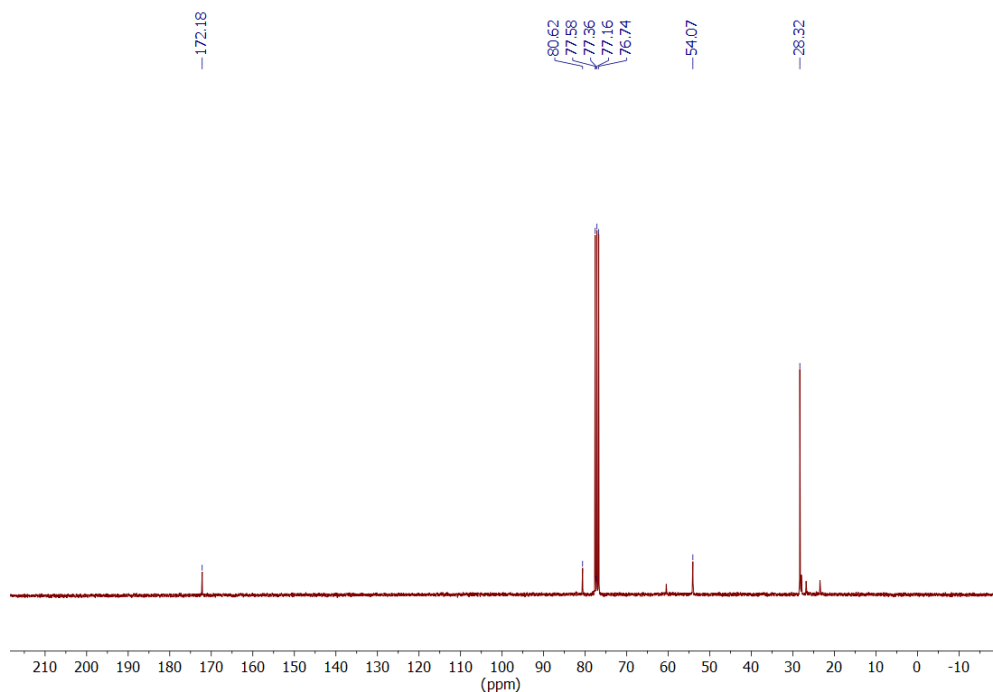


Figure S8: ¹³C NMR spectrum of compound **2** (75 MHz, CDCl₃, 298 K).

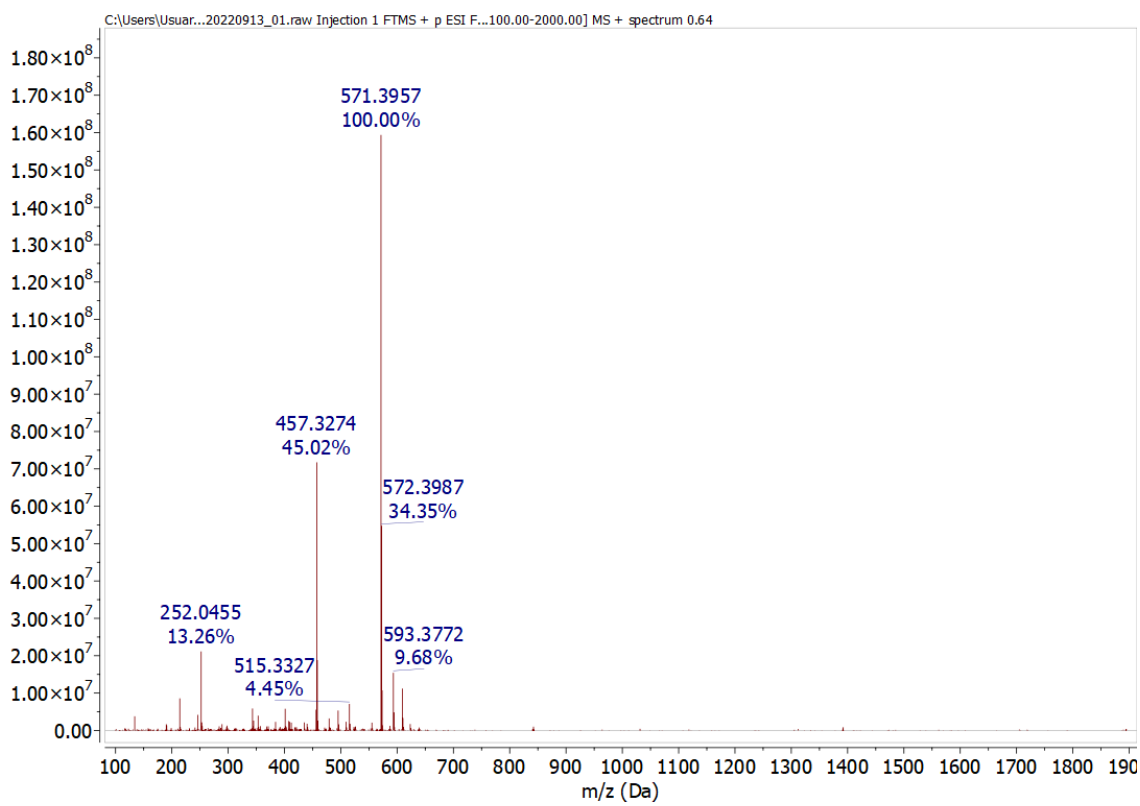


Figure S9: Experimental high resolution mass spectrum (ESI^+) of compound **2**.

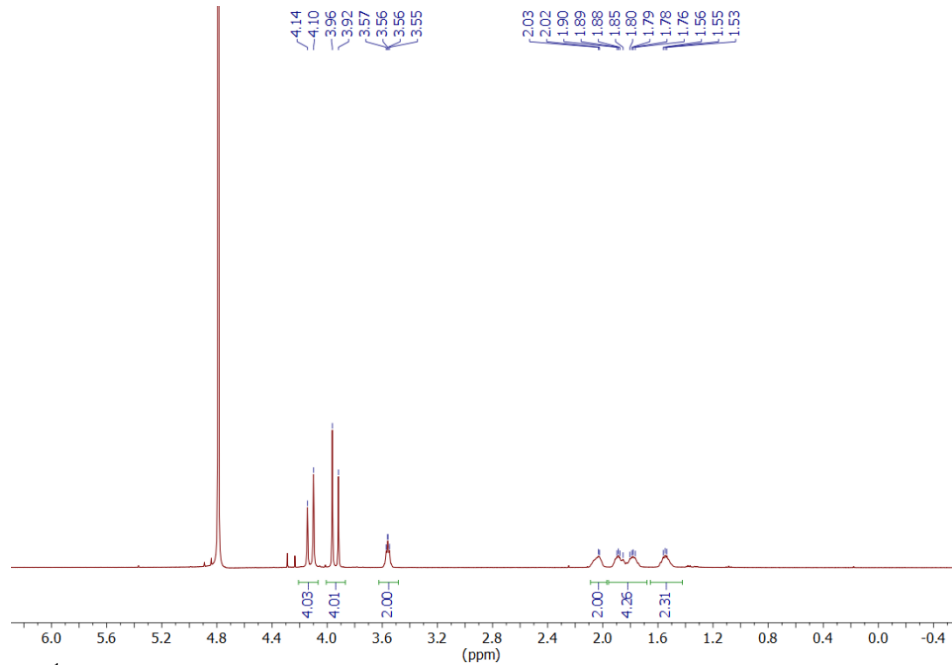


Figure S10: ^1H NMR spectrum of **1,2-c-H₄CDTA** (300 MHz, D_2O , 298 K, pH 1).

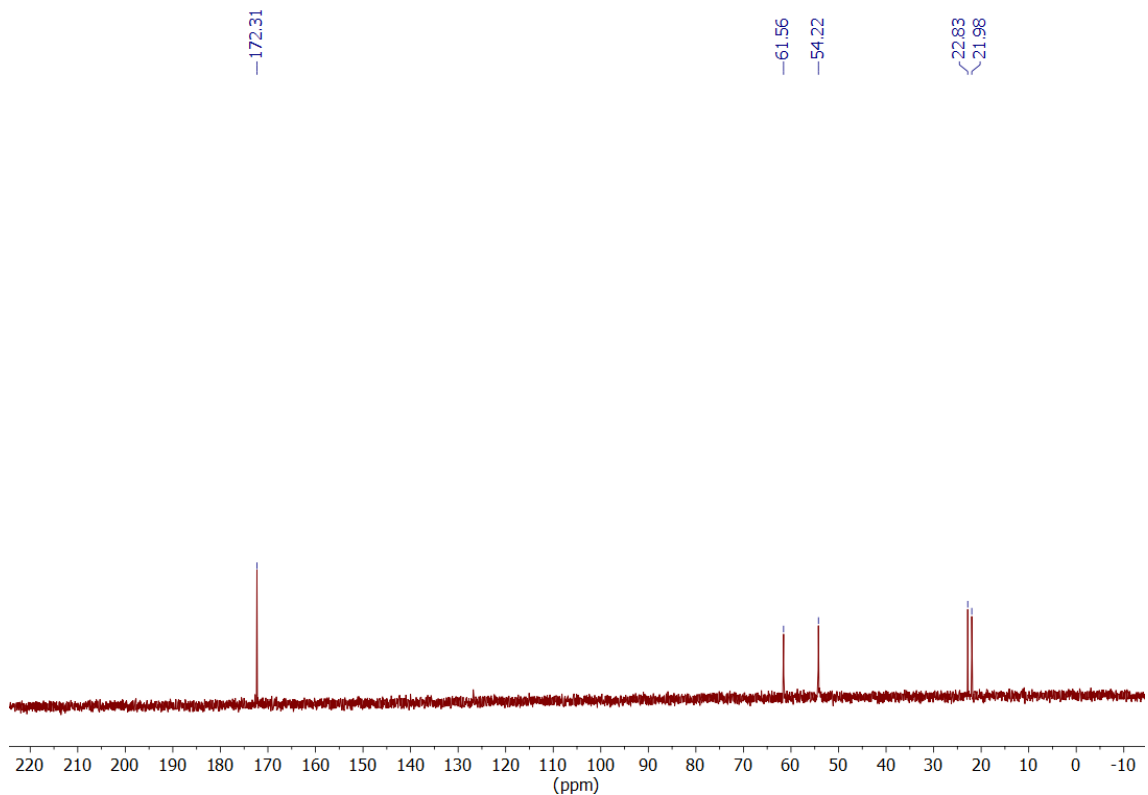


Figure S11: ^{13}C NMR spectrum of **1,2-c-H₄CDTA** (75 MHz, D₂O, 298 K, pH 1).

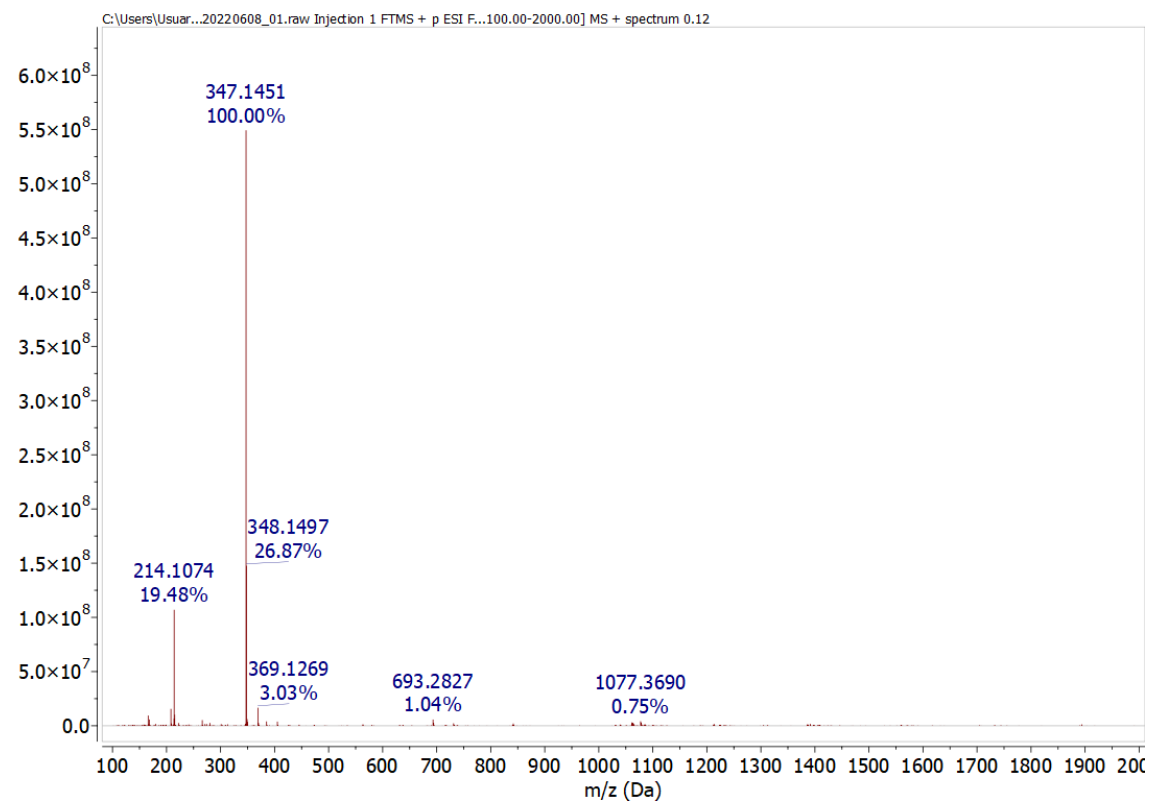
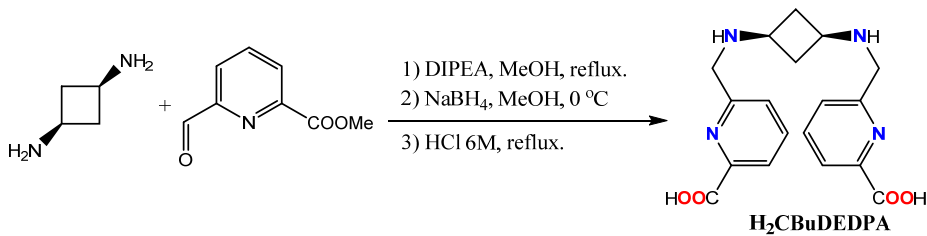


Figure S12: Experimental high resolution mass spectrum (ESI $^+$) of **1,2-c-H₄CDTA**.



Scheme S3: Synthesis of **H₂CBuDEDPA**.

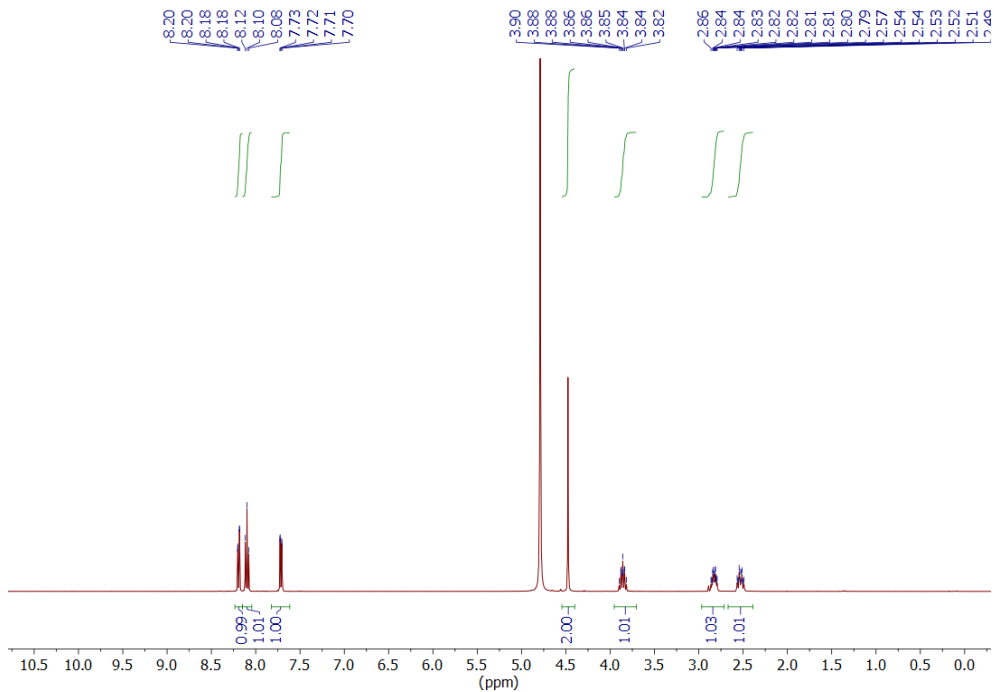


Figure S13: ¹H NMR spectrum of **H₂CBuDEDPA** (400 MHz, D₂O, pH 2, 298 K).

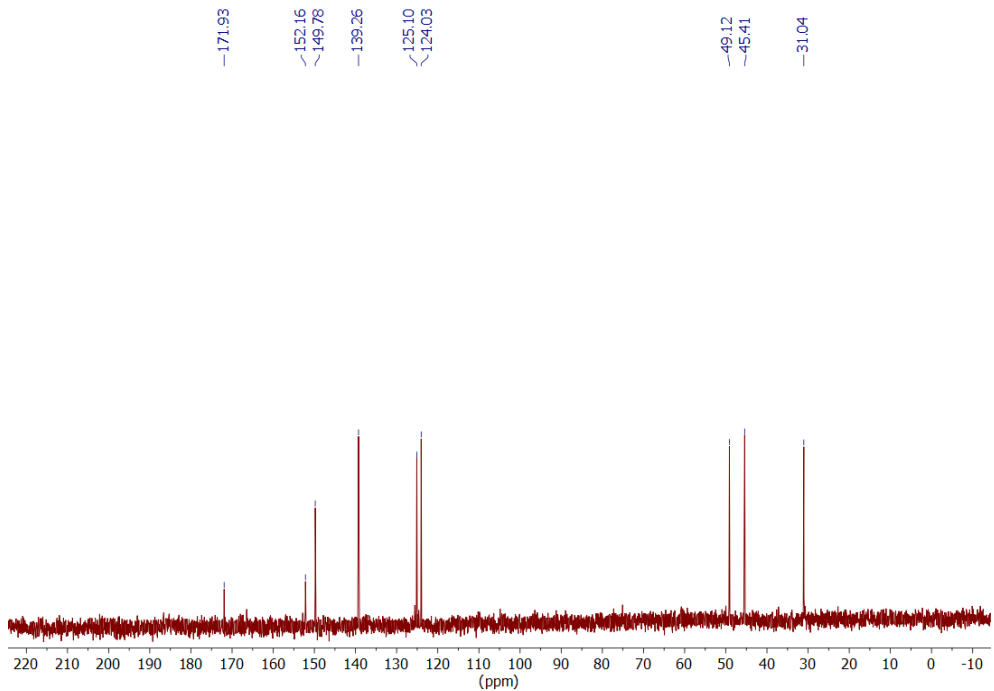


Figure S14: ¹³C NMR spectrum of **H₂CBuDEDPA** (400 MHz, D₂O, pH 2, 298 K).

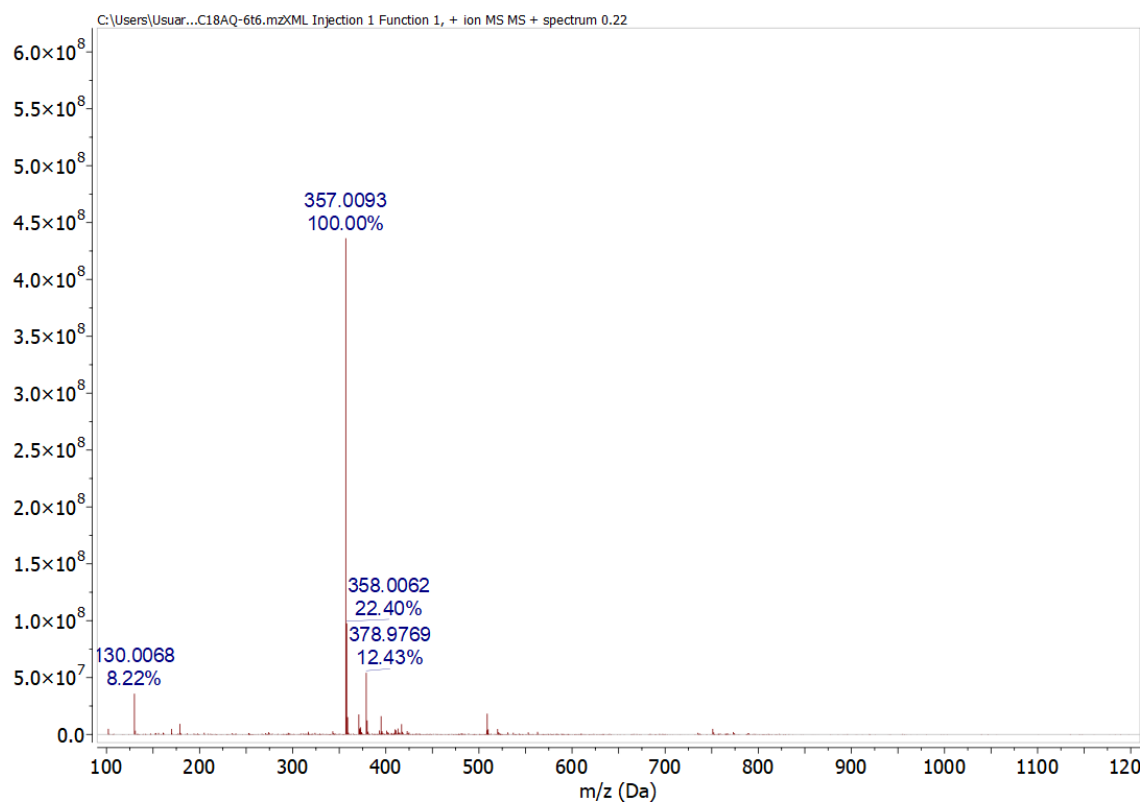


Figure S15: Experimental high resolution mass spectrum (ESI^+) of $\text{H}_2\text{CBuDEDPA}$.

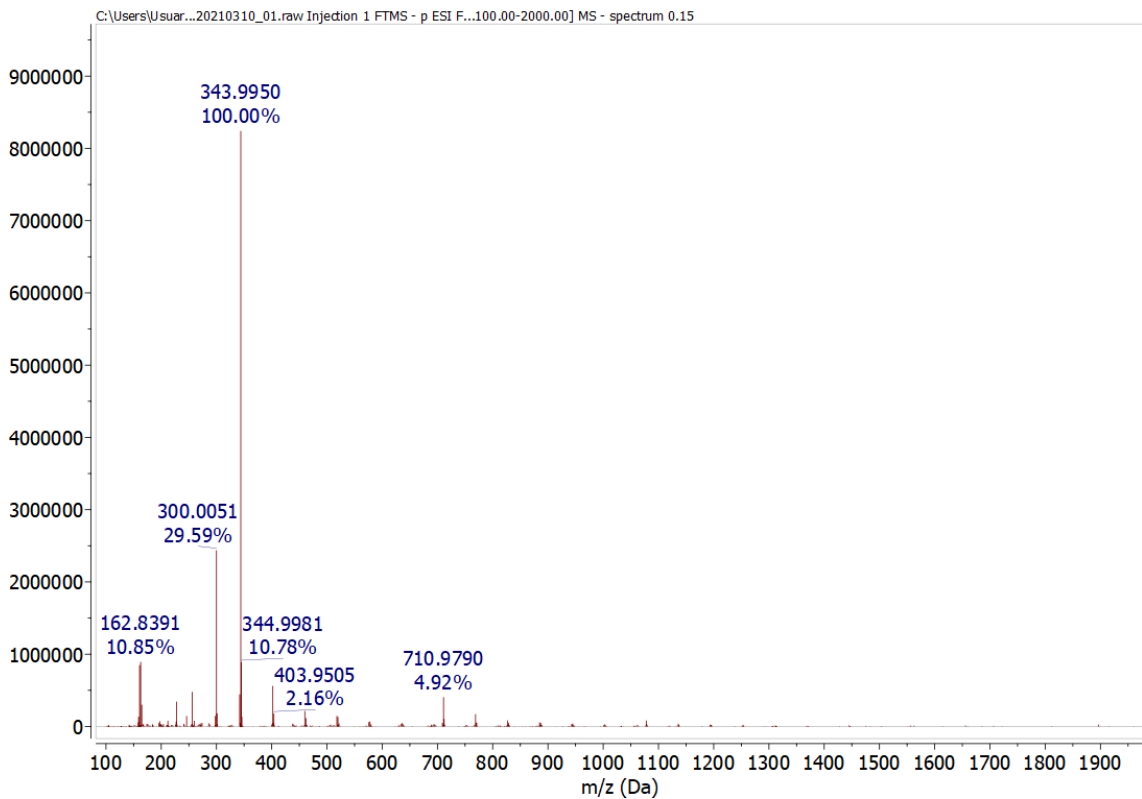


Figure S16: Experimental high resolution mass spectrum (ESI^+) of $[\text{Fe}(\text{EDTA})]^-$.

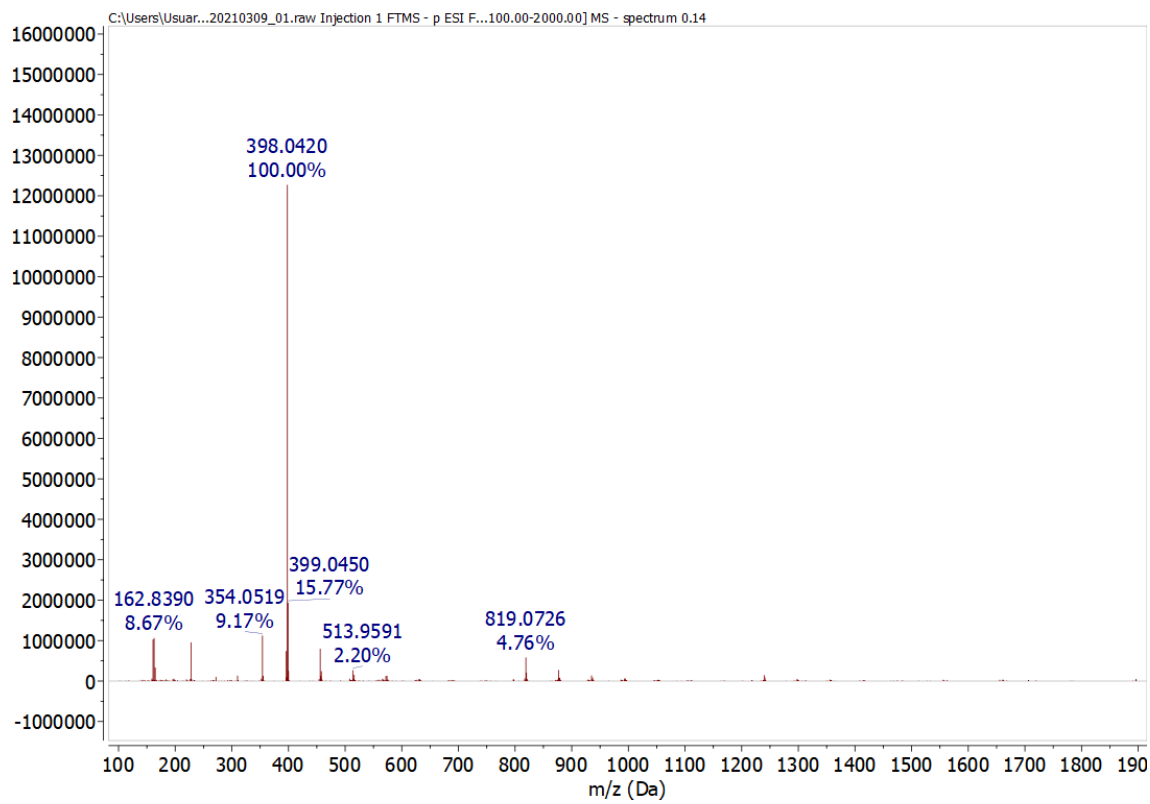


Figure S17: Experimental high resolution mass spectrum (ESI^+) of $[\text{Fe}(t\text{-CDTA})]^-$.

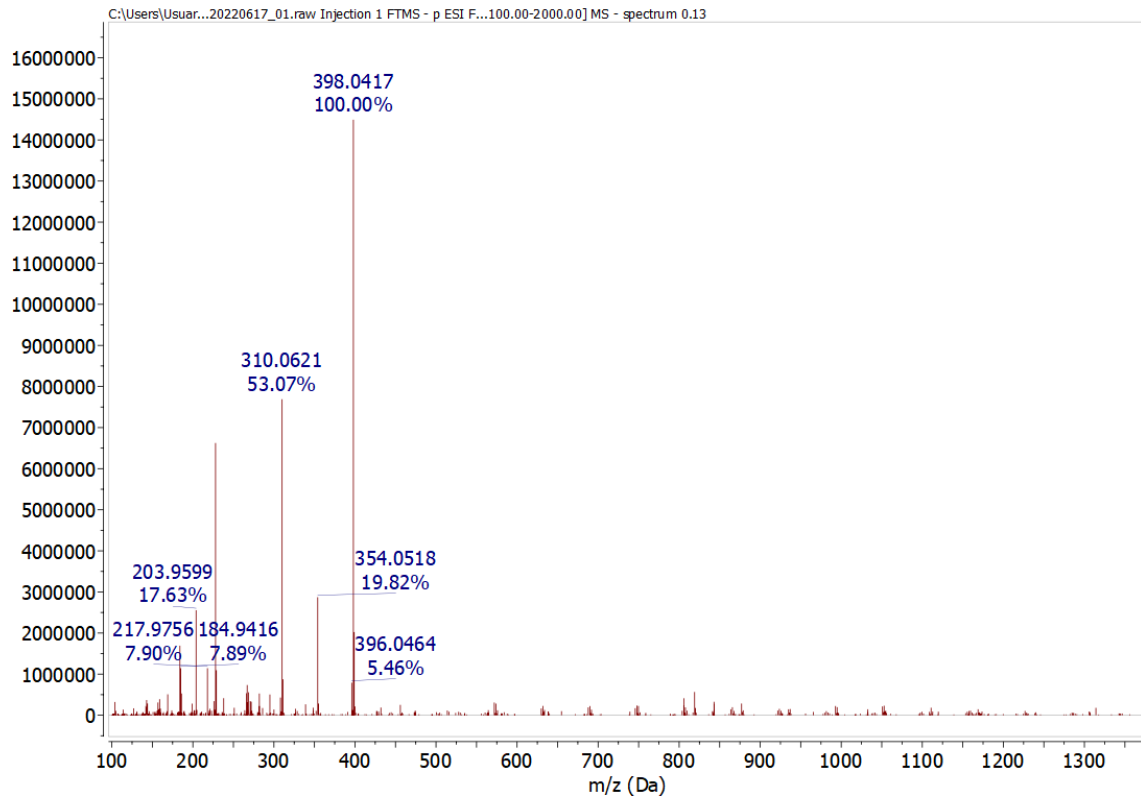


Figure S18: Experimental high resolution mass spectrum (ESI^+) of $[\text{Fe}(c\text{-CDTA})]^-$.

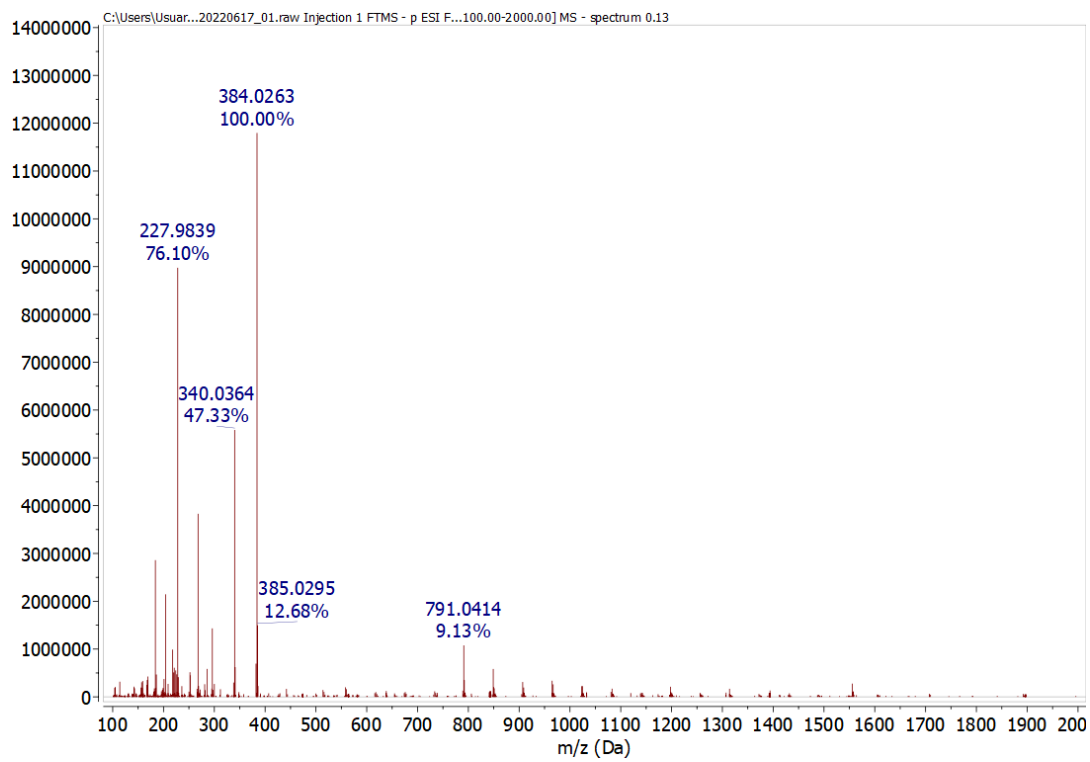


Figure S 19: Experimental high resolution mass spectrum (ESI^+) of $[\text{Fe}(\text{CpDTA})]^-$.

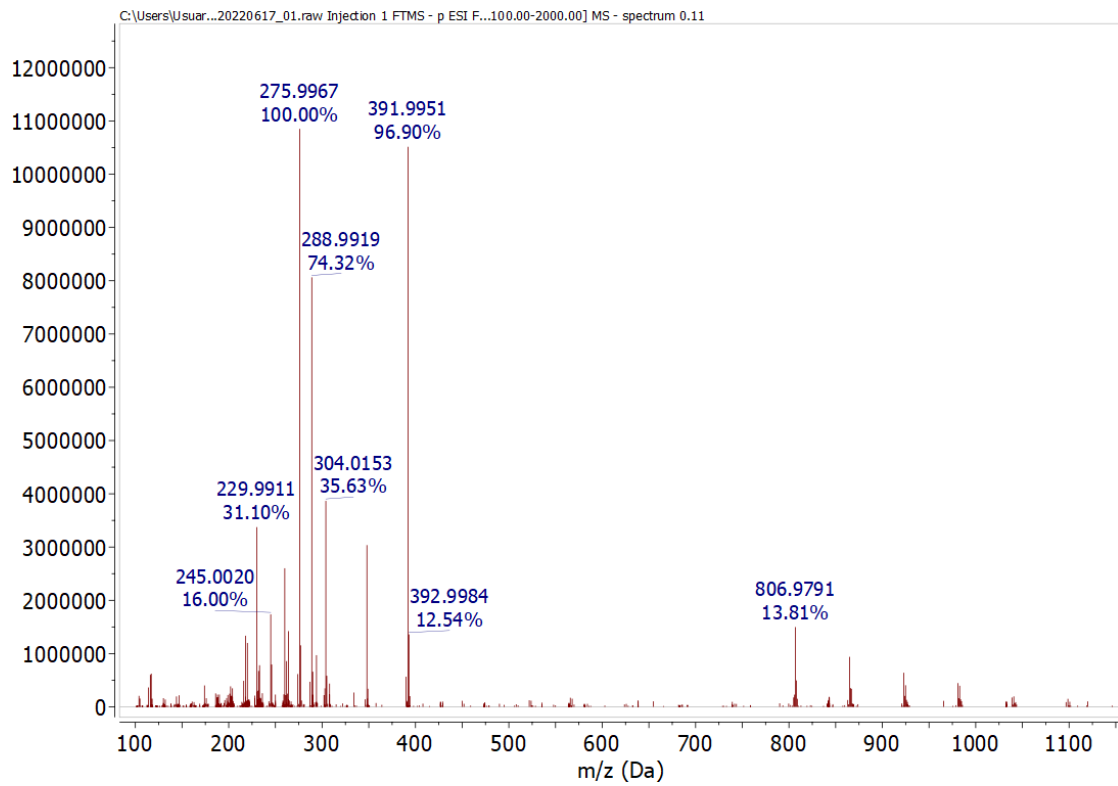


Figure S 20: Experimental high resolution mass spectrum (ESI^+) of $[\text{Fe}(\text{PhDTA})]^-$.

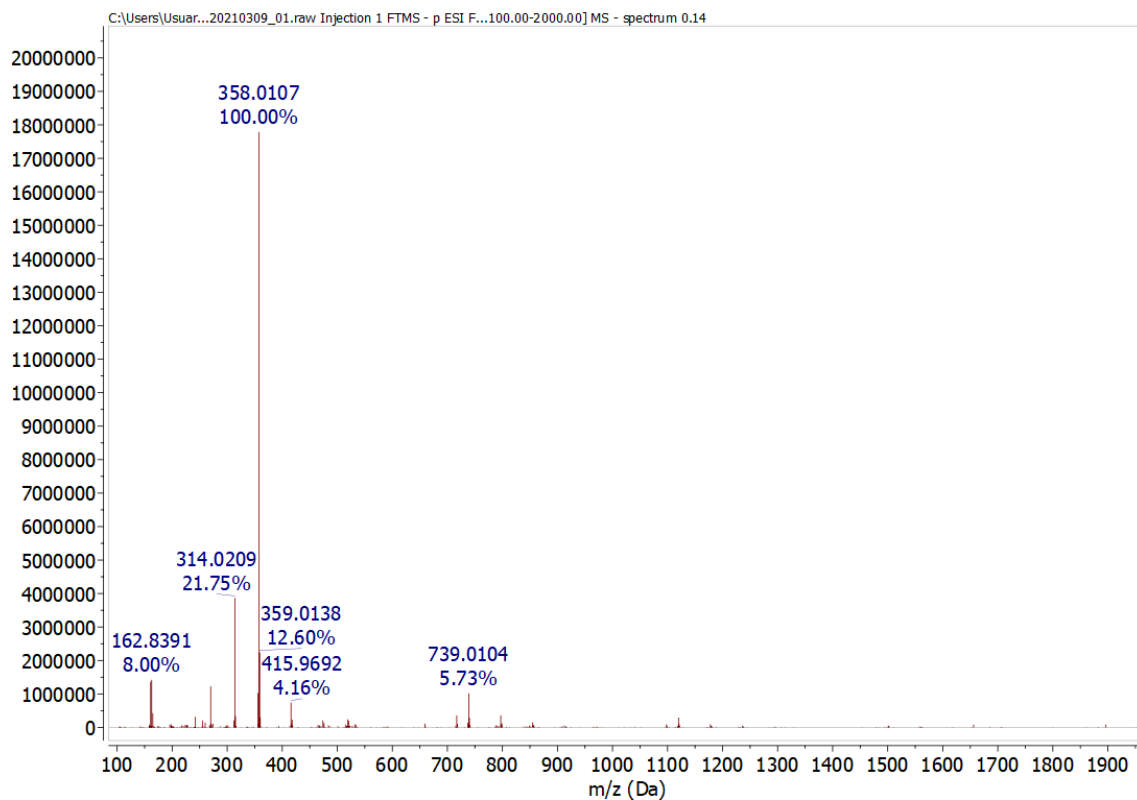


Figure S21: Experimental high resolution mass spectrum (ESI^+) of $[\text{Fe}(\text{PDTA})]^-$.

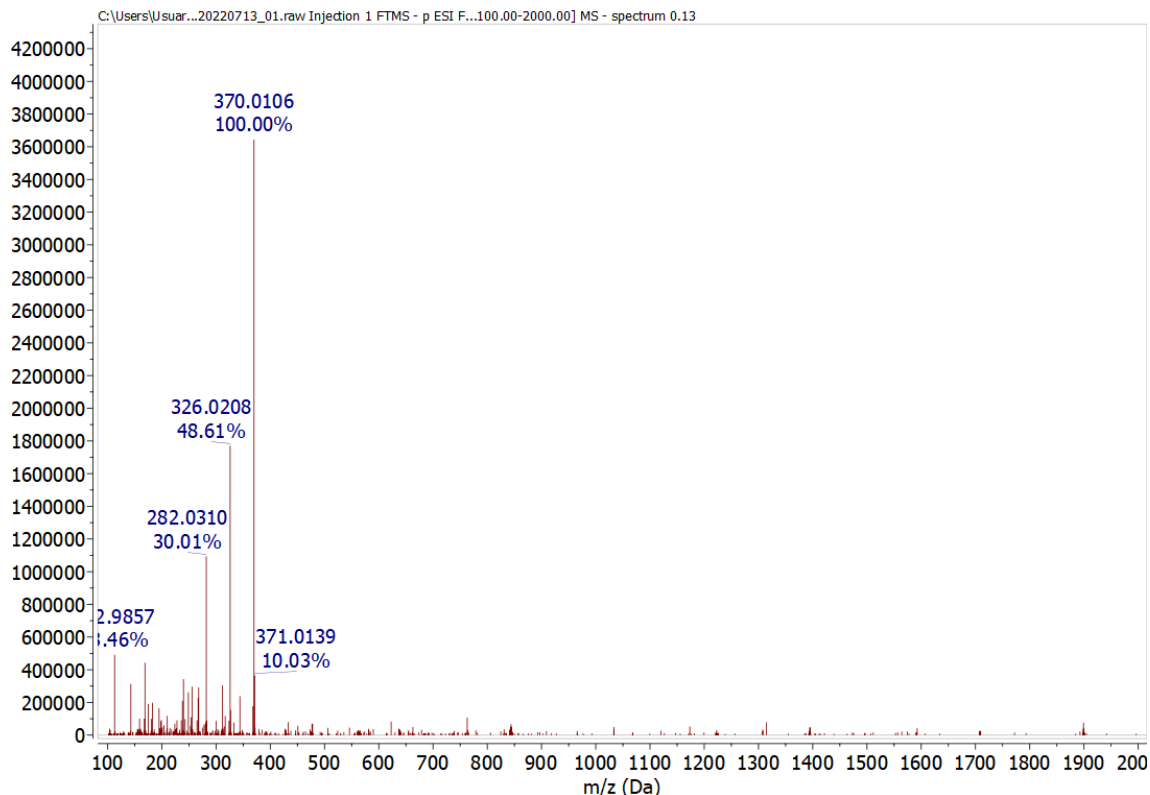


Figure S22: Experimental high resolution mass spectrum (ESI^+) of $[\text{Fe}(\text{CBuDTA})]^-$.

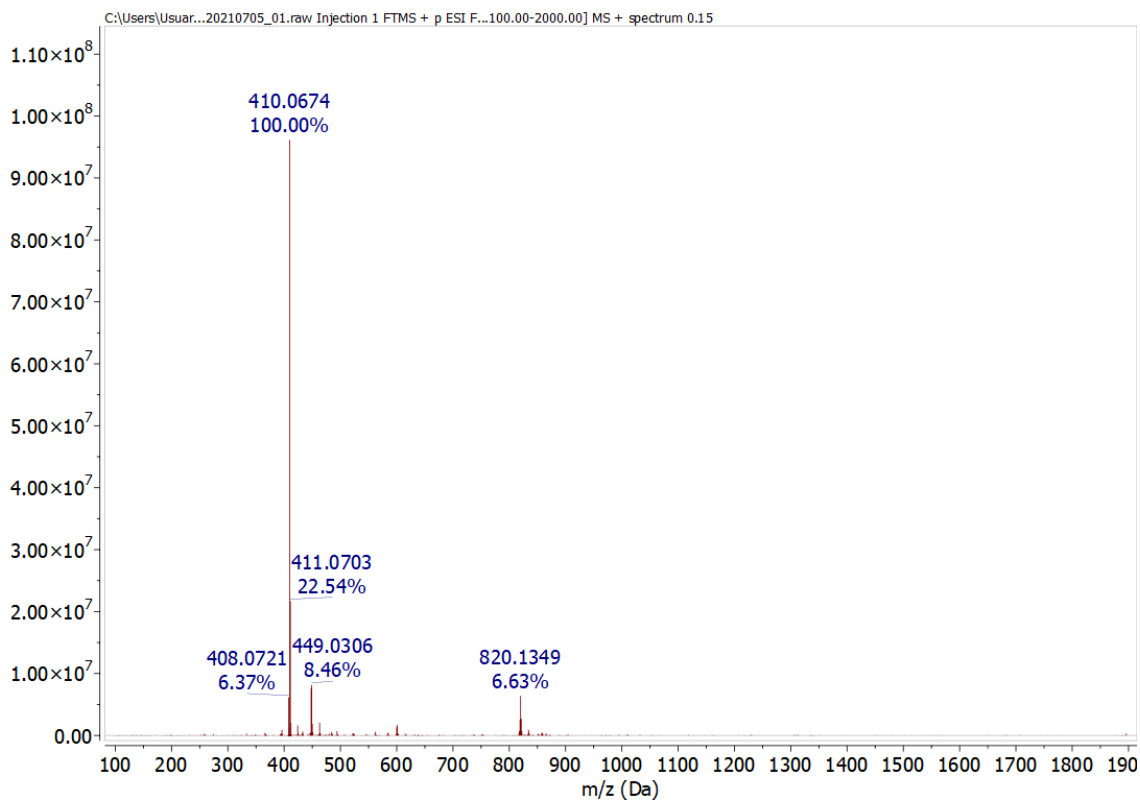


Figure S23: Experimental high resolution mass spectrum (ESI^+) of $[\text{Fe}(\text{CBuDEDPA})]^+$.

Table S1: Crystal Data and Structure Refinement Details. Parameter $[\text{Fe}(\text{CBuDEDPA})](\text{PF}_6)$.

Empirical formula	$[\text{Fe}(\text{C}_{18}\text{H}_{20}\text{N}_4\text{O}_5]\text{PF}_6$
Molecular weight MW	573.20
Crystal system	Monoclinic
Space group	$P2_1/n$
a/\AA	12.4135(5)
b/\AA, $\beta/^\circ$	10.9733(4), 93.6190(10)
c/\AA	15.5664(6)
Volume (\AA^3)	2116.18(14)
Z	4
ρ_{calc} (g/cm³)	1.799
μ (mm⁻¹)	0.883
θ range	2.48°-28.31°
R_{int}	0.0310
Measured reflections	43559
Independent reflections / unique ($I > 2\sigma(I)$)	5254 / 4893
Goodness-of-fit on F^2	1.092
R_1	0.0298
wR₂ (all data)	0.0710
Larg. diff. peak and hole (e\AA^{-3})	0.45 and -0.35

Cyclic voltammetry

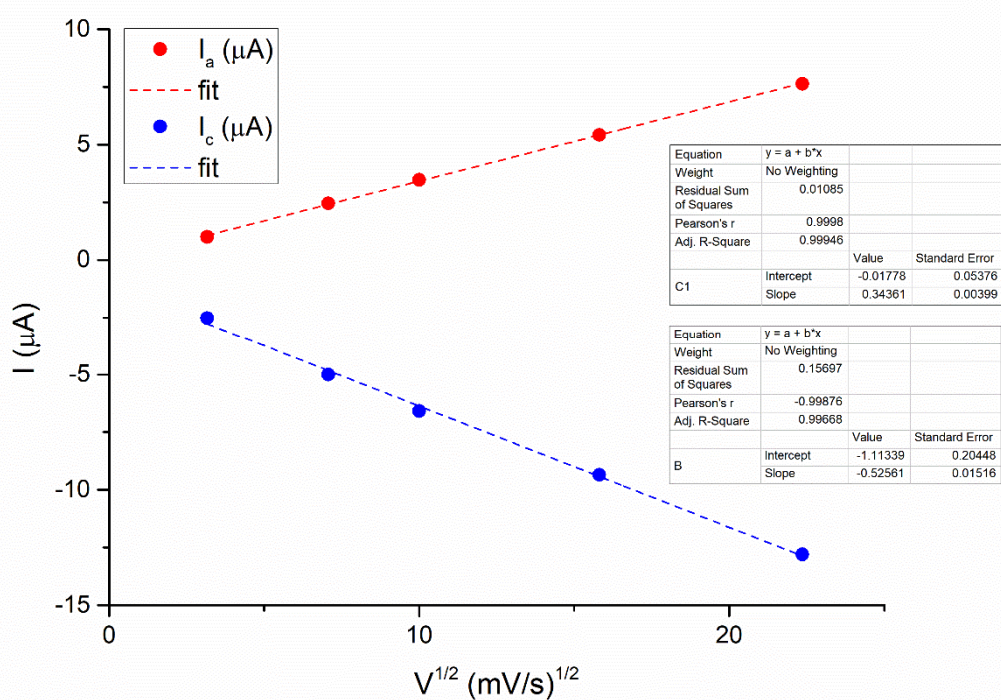
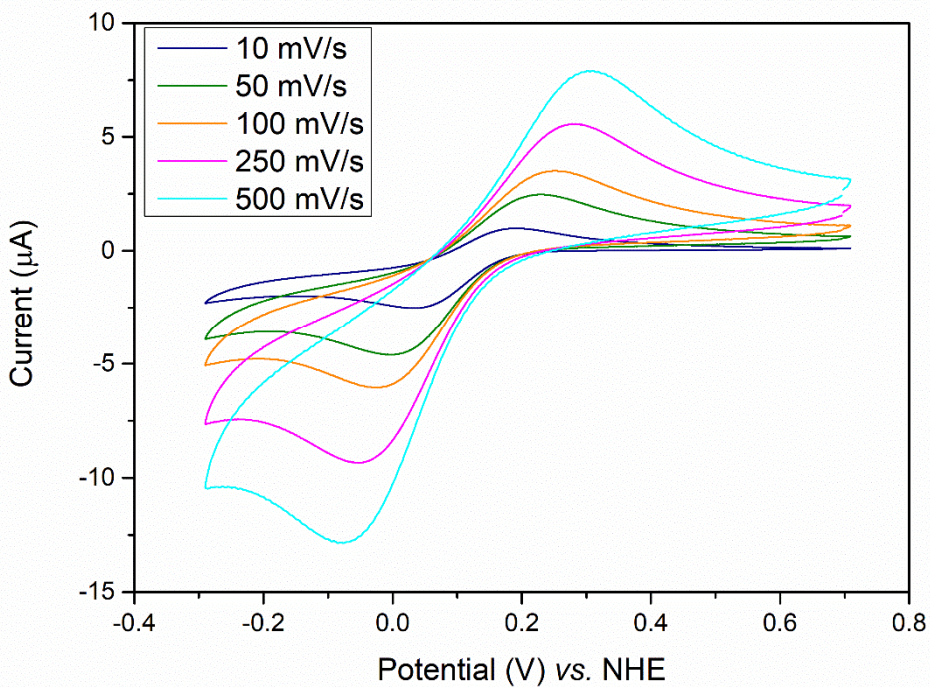


Figure S24: Cyclic voltammogram of $[\text{Fe}(\text{EDTA})]^-$ complex in aqueous solution in 0.15 M NaCl (2.6 mM, pH= 5.5), recorded at 10, 50, 100, 250, and 500 $\text{mV}\cdot\text{s}^{-1}$ (top); and plots of the linear dependence of anodic and cathodic peak currents with the square root of the scan rate (bottom).

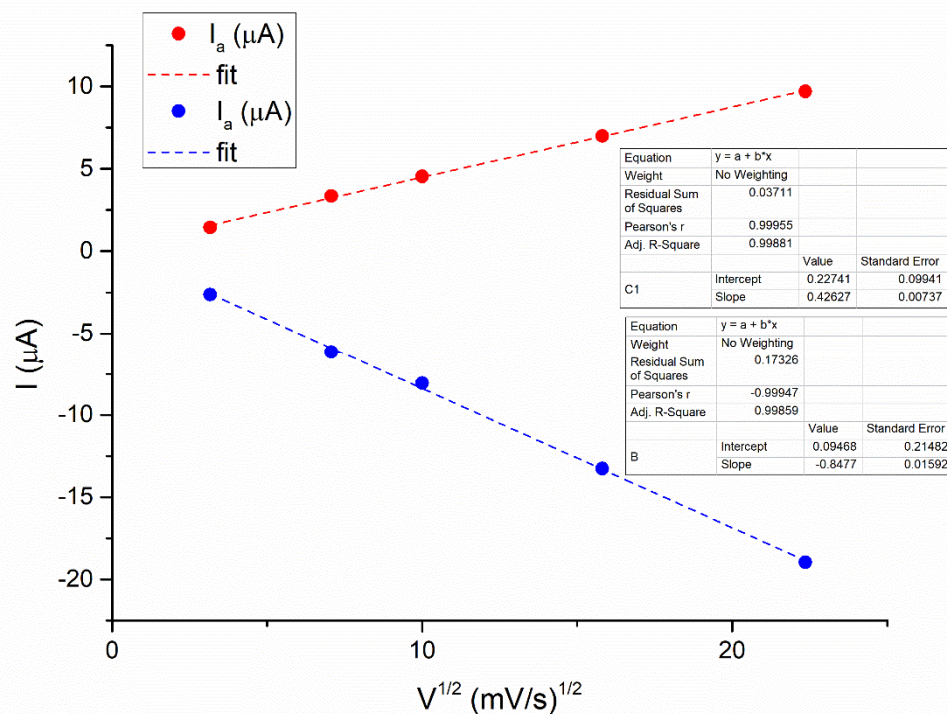
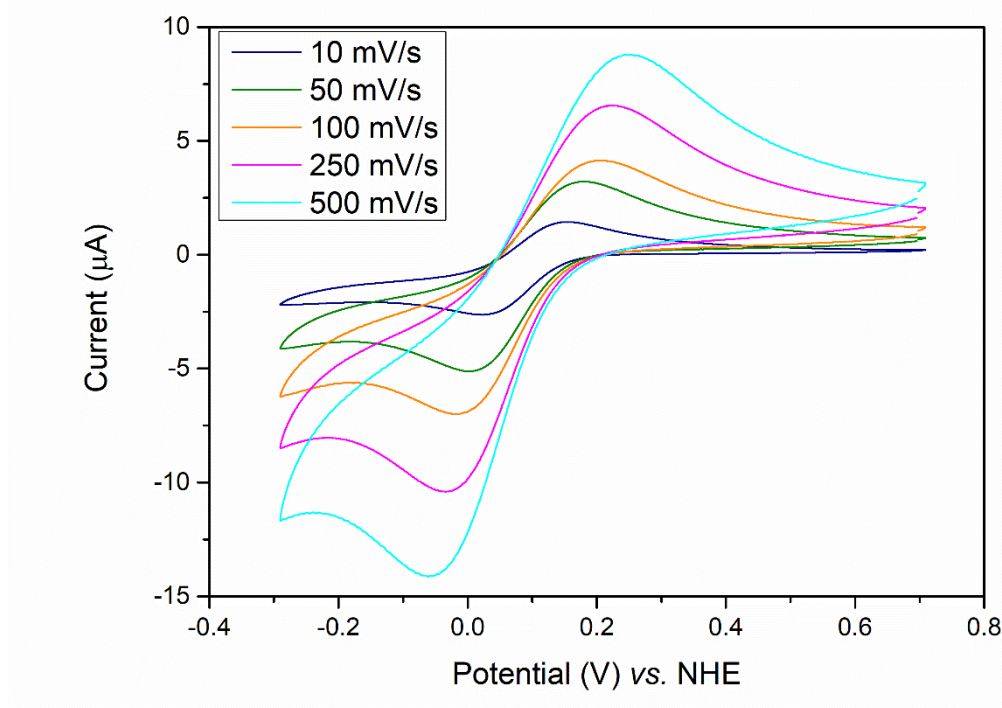


Figure S25: Cyclic voltammogram of $[\text{Fe}(t\text{-CDTA})]^-$ complex in aqueous solution in 0.15 M NaCl (2.6 mM, pH= 5.3), recorded at 10, 50, 100, 250, and 500 $\text{mV}\cdot\text{s}^{-1}$ (top); and plots of the linear dependence of anodic and cathodic peak currents with the square root of the scan rate (bottom).

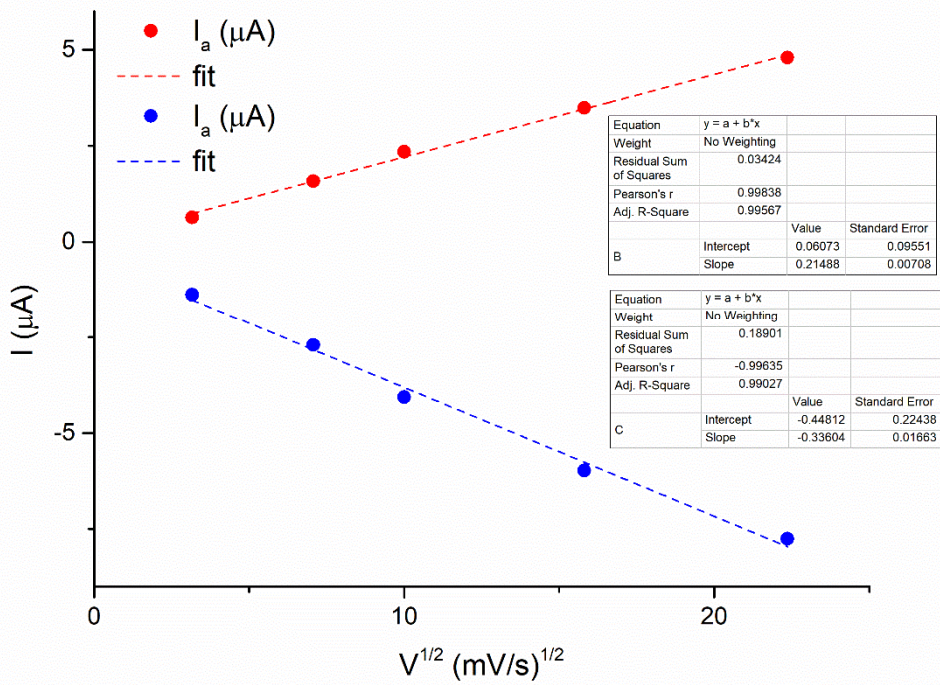
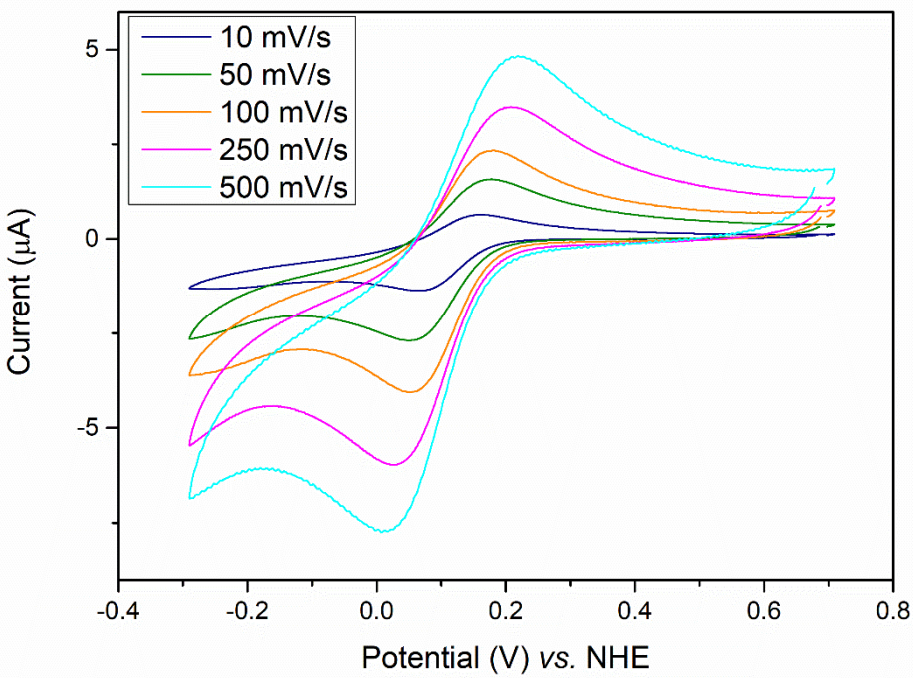


Figure S26: Cyclic voltammogram of $[\text{Fe(c-CDTA)}]^-$ complex in aqueous solution in 0.15 M NaCl (2.0 mM, pH= 6.8), recorded at 10, 50, 100, 250, and 500 $\text{mV}\cdot\text{s}^{-1}$ (top); and plots of the linear dependence of anodic and cathodic peak currents with the square root of the scan rate (bottom).

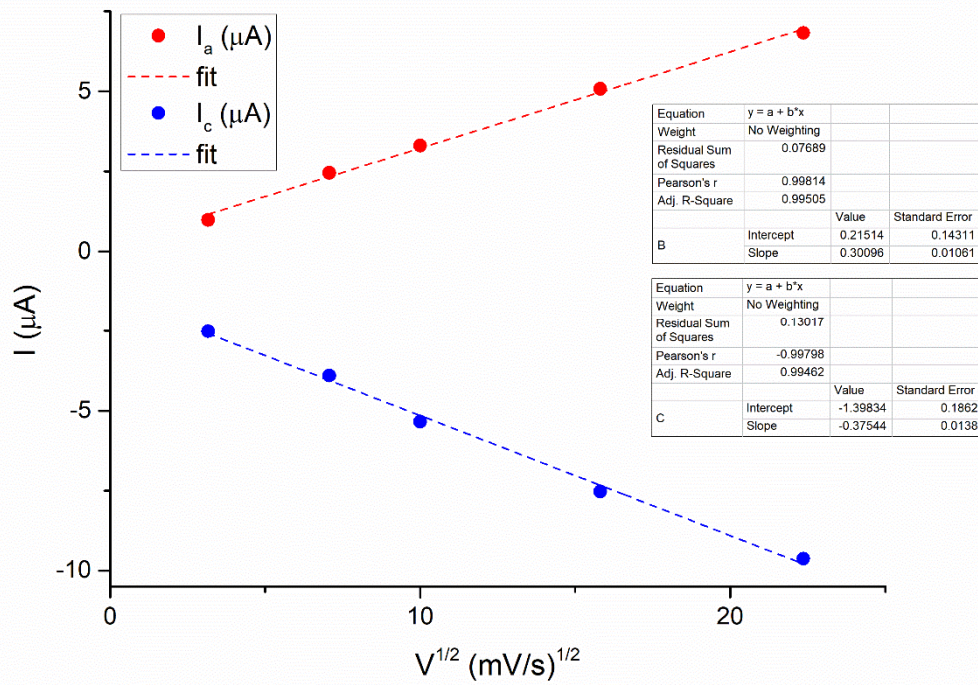
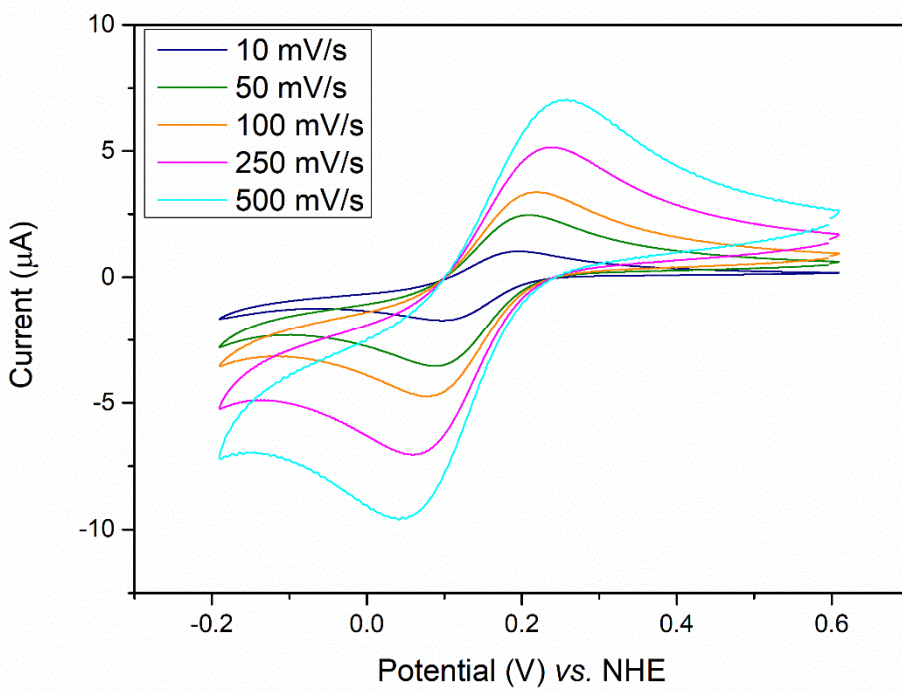


Figure S27: Cyclic voltammogram of $[\text{Fe}(\text{CpDTA})]^-$ complex in aqueous solution in 0.15 M NaCl (2.0 mM, pH= 5.7), recorded at 10, 50, 100, 250, and 500 $\text{mV}\cdot\text{s}^{-1}$ (top); and plots of the linear dependence of anodic and cathodic peak currents with the square root of the scan rate (bottom).

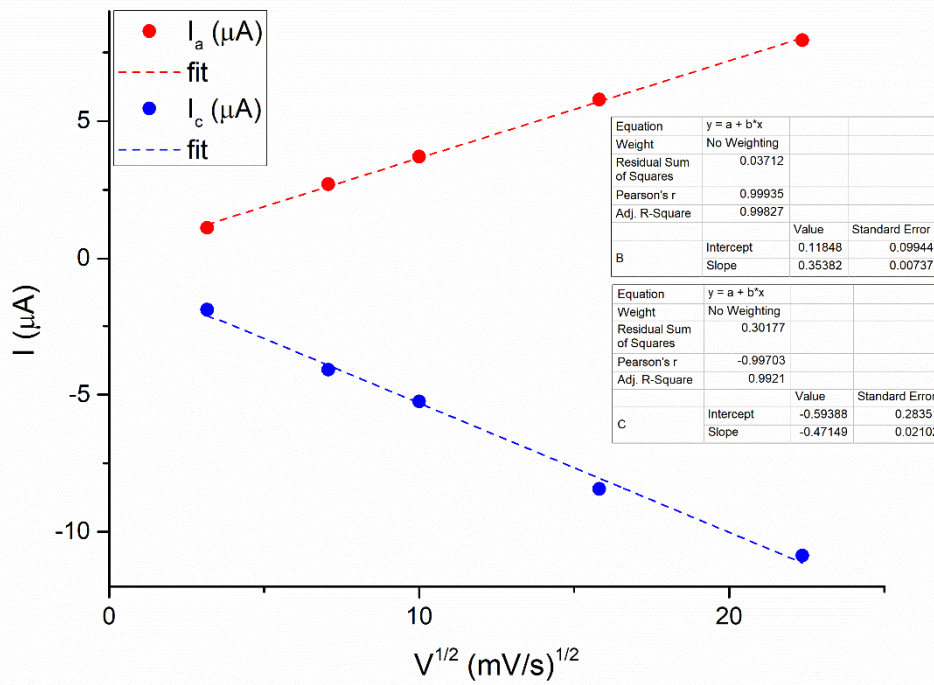
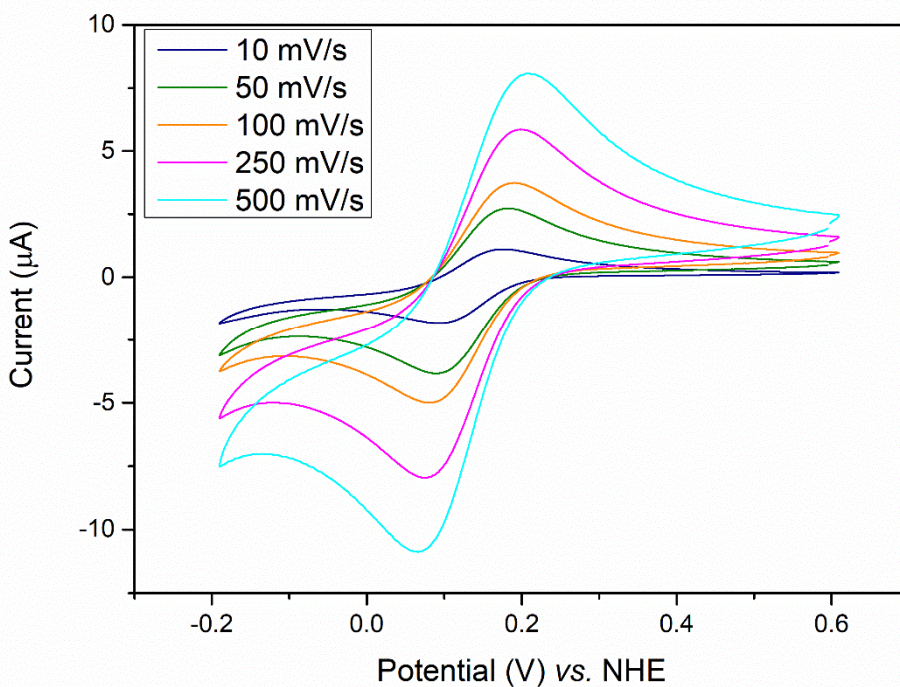


Figure S28: Cyclic voltammogram of $[\text{Fe}(\text{PhDTA})]^-$ complex in aqueous solution in 0.15 M NaCl (2 mM, pH= 5.6), recorded at 10, 50, 100, 250, and 500 $\text{mV} \cdot \text{s}^{-1}$ (top); and plots of the linear dependence of anodic and cathodic peak currents with the square root of the scan rate (bottom).

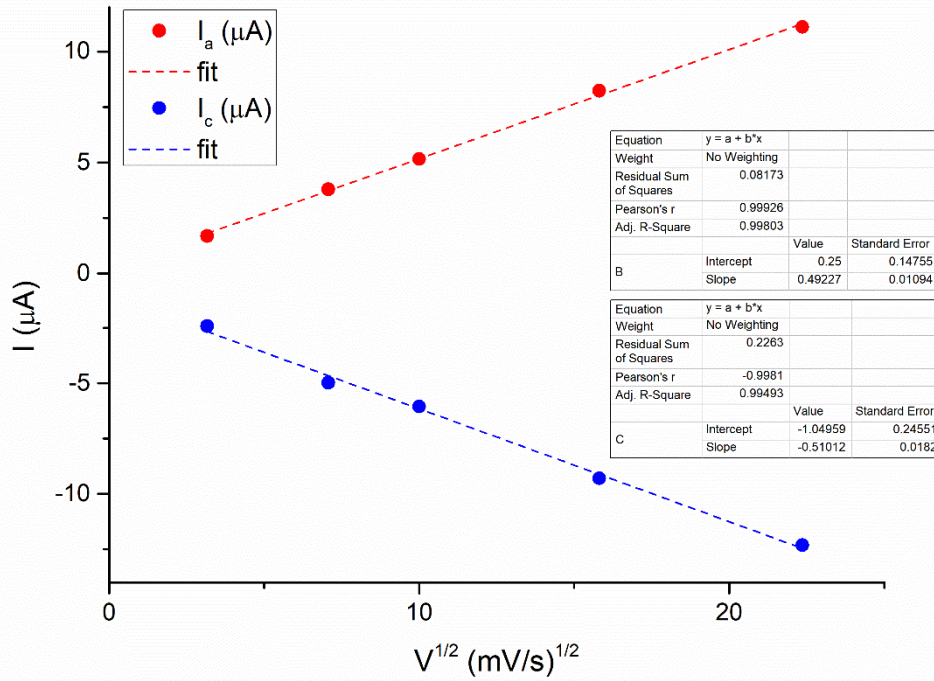
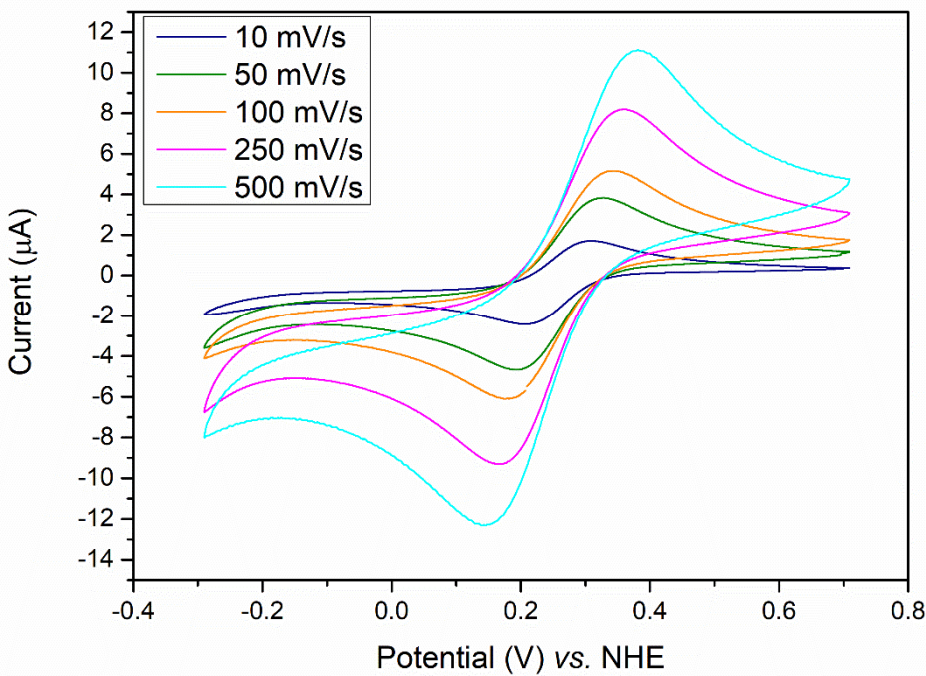


Figure S29: Cyclic voltammogram of $[\text{Fe}(\text{PDTA})]^-$ complex in aqueous solution in 0.15 M NaCl (3.0 mM, pH= 5.9), recorded at 10, 50, 100, 250, and 500 $\text{mV}\cdot\text{s}^{-1}$ (top); and plots of the linear dependence of anodic and cathodic peak currents with the square root of the scan rate (bottom).

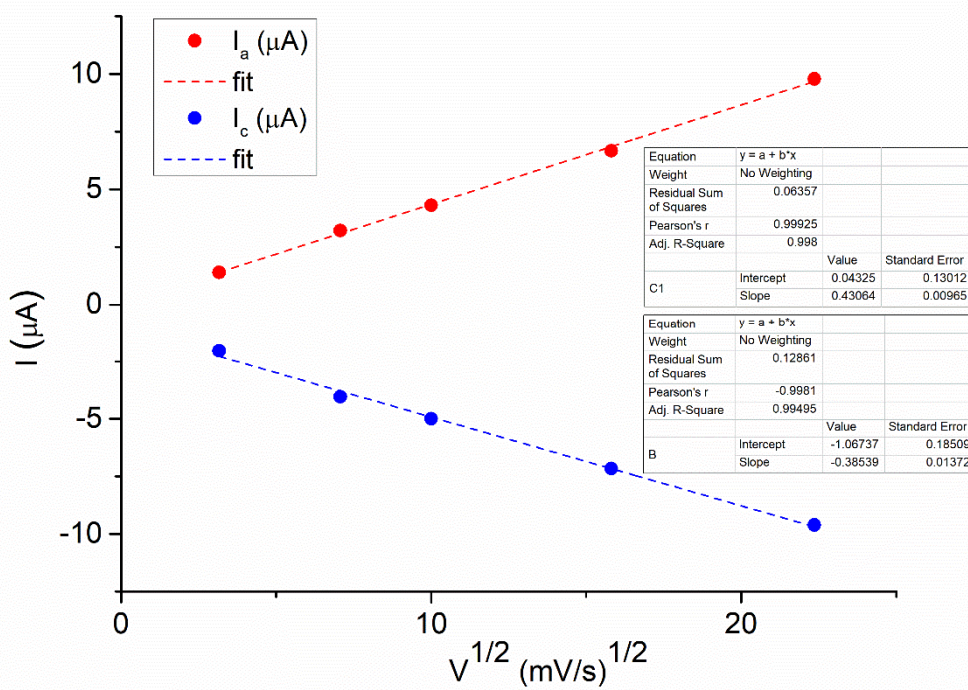
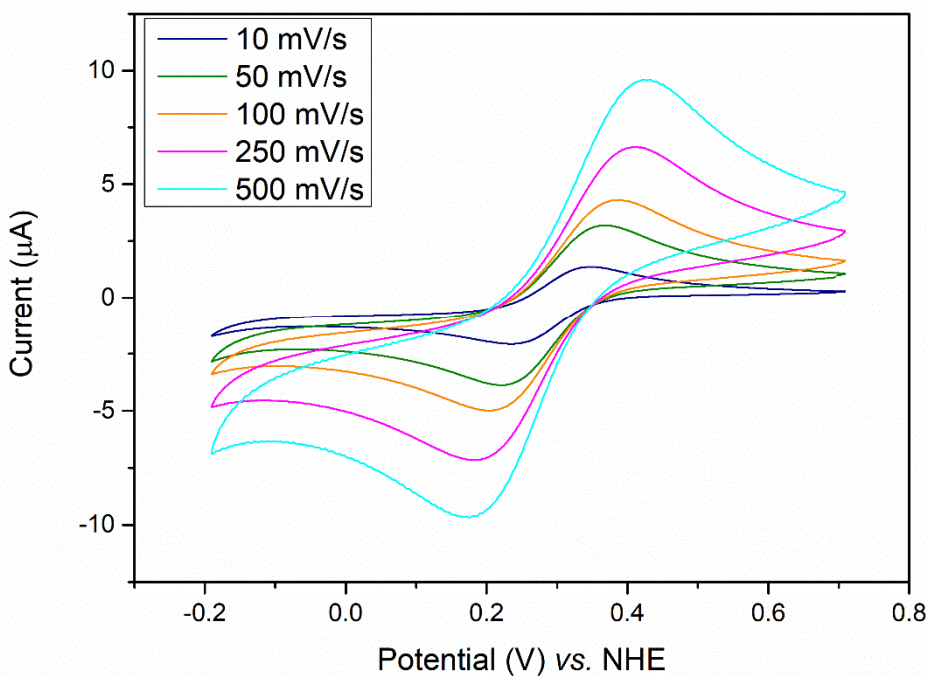


Figure S30: Cyclic voltammogram of $[\text{Fe(CBuDTA)}]^-$ complex in aqueous solution in 0.15 M NaCl (2.3 mM, pH= 5.7), recorded at 10, 50, 100, 250, and 500 $\text{mV} \cdot \text{s}^{-1}$ (top); and plots of the linear dependence of anodic and cathodic peak currents with the square root of the scan rate (bottom).

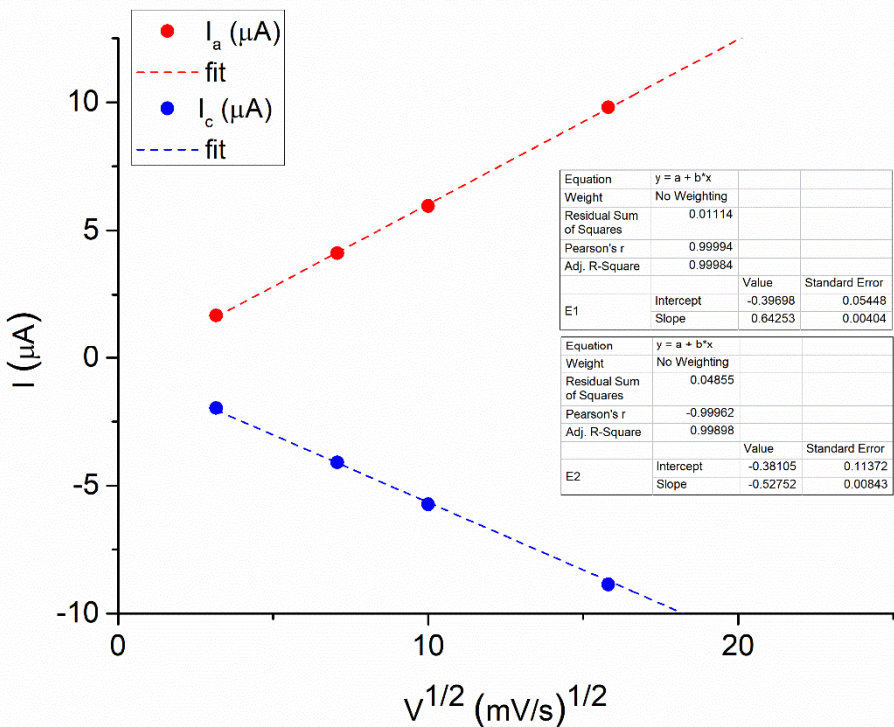
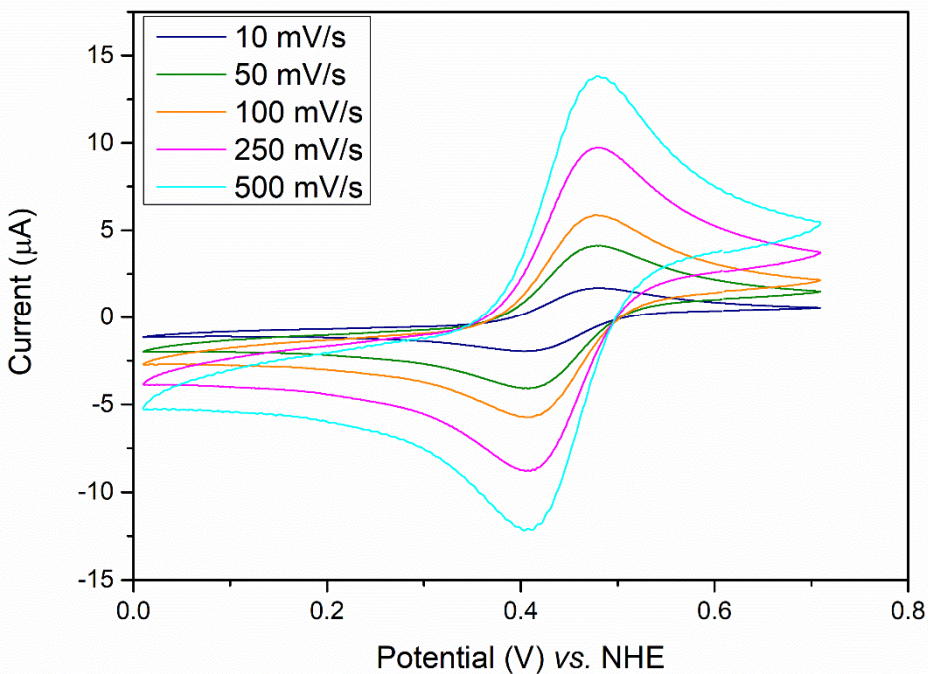


Figure S31: Cyclic voltammogram of $[\text{Fe}(\text{CBuDEDPA})]^+$ complex in aqueous solution in 0.15 M NaCl (1.5 mM, pH= 5.1), recorded at 10, 50, 100, 250, and 500 $\text{mV}\cdot\text{s}^{-1}$ (top); and plots of the linear dependence of anodic and cathodic peak currents with the square root of the scan rate (bottom).

28	1	-0.514106	-0.284069	-2.788032
29	1	-1.935775	-1.326325	-2.814638
30	6	-2.092486	0.421451	-1.557489
31	8	-0.474173	1.718936	1.730866
32	1	0.106286	1.977960	2.471245
33	1	-0.688568	2.529005	1.215476
34	8	-0.727250	3.795056	0.016167
35	8	1.371339	2.133222	3.736411
36	1	-0.171777	3.234638	-0.545239
37	1	-1.611694	3.769013	-0.394750
38	1	1.102421	1.769204	4.580202
39	1	1.742835	1.386618	3.230681
40	26	0.260516	0.226672	0.394770
41	8	-3.961809	0.677968	1.306388
42	1	-3.160448	0.784254	0.777408
43	1	-4.158504	-0.270033	1.295631
44	8	-4.553655	-2.120099	1.439793
45	8	-3.242672	3.593264	-1.148318
46	1	-3.131047	2.708043	-1.552320
47	1	-3.381314	4.194457	-1.880111
48	1	-4.937552	-2.545226	0.673038
49	1	-3.688452	-2.543718	1.572043
50	6	0.998238	-1.907359	-2.853431
51	6	2.185040	-2.822275	-1.486432
52	1	2.574338	-3.054907	-0.517293
53	1	2.510560	-3.424696	-2.308640
54	1	1.376953	-2.698009	-3.466903
55	1	0.418327	-1.158720	-3.351569

Zero-point correction=	0.430168 (Hartree/Particle)
Thermal correction to Energy=	0.466168
Thermal correction to Enthalpy=	0.467113
Thermal correction to Gibbs Free Energy=	0.361580
Sum of electronic and zero-point Energies=	-2899.529010
Sum of electronic and thermal Energies=	-2899.493010
Sum of electronic and thermal Enthalpies=	-2899.492066
Sum of electronic and thermal Free Energies=	-2899.597598

References

- 1 J. M. Wilson and R. F. Carbonaro, Capillary electrophoresis study of iron(II) and iron(III) polyaminocarboxylate complex speciation, *Environ. Chem.*, 2011, **8**, 295–303.